

Initial and Final State Interaction Effects in Small- x Quark Distributions

Bo-Wen Xiao¹ and Feng Yuan^{1,2}

¹*Nuclear Science Division, Lawrence Berkeley National Laboratory, Berkeley, CA 94720*

²*RIKEN BNL Research Center, Building 510A,
Brookhaven National Laboratory, Upton, NY 11973*

Abstract

We study the initial and final state interaction effects in the transverse momentum dependent parton distributions in the small- x saturation region. In particular, we discuss the quark distributions in the semi-inclusive deep inelastic scattering, Drell-Yan lepton pair production and dijet-correlation processes in pA collisions. We calculate the quark distributions in the scalar-QED model and then extend to the color glass condensate formalism in QCD. The quark distributions are found universal between the DIS and Drell-Yan processes. On the other hand, the quark distribution from the $qq' \rightarrow qq'$ channel contribution to the dijet-correlation process is not universal. However, we find that it can be related to the quark distribution in DIS process by a convolution with the normalized unintegrated gluon distribution in the color glass condensate formalism in the large N_c limit.

I. INTRODUCTION

Partonic internal structure of nucleon and nucleus have attracted many theoretical and experimental investigations in the past and are still in the frontier of the subatomic physics research. These studies aim at providing us accurate description of the hadronic structure in terms of fundamental degree of freedom in Quantum Chromodynamics (QCD), and meanwhile presenting an important path to discover the new physics beyond the Standard Model, which are currently undertaken at various high energy experiments, such as the Fermilab Tevatron, and the Large Hadron Collider at CERN. One of the most important objects is the parton distribution functions (PDFs). These functions describe the internal structure of hadrons in terms of the distribution of the longitudinal momentum fraction x carried by partons in the infinite momentum frame and the relevant QCD factorization has been well developed [1].

In recent years, hadronic physics community have extended the Feynman parton distributions to include the dependence on additional dimensions, in particular in the transverse directions perpendicular to the parenting hadron momentum direction. These extensions appear in two different fashions: in the transverse coordinate space as the generalized parton distributions (GPDs) [2]; in the transverse momentum space as the transverse momentum dependent parton distributions (TMDs) [3]. A number of experimental facilities, such as the 12GeV upgrade of Jefferson Lab, the Relativistic Heavy Ion Collider at the Brookhaven National Lab, and the planned Electron-Ion Collider, are trying to measure these distribution functions. These studies will lead us to the final answers to the important questions concerning the nucleon (nucleus) structure: the proton spin and parton saturation in nucleon (nucleus) at small x .

Transverse momentum dependence in the parton distributions is also crucial to understand some novel hadronic physics phenomena in high energy scattering processes. This includes, for example, the single transverse spin asymmetries [4–7] and small- x saturation phenomena [8, 9]. In the case for the small- x physics, the so-called k_t -dependent parton distributions contain resummation effects which come from multiple scattering associated with the nucleus target. Phenomenologically, the k_t -dependent gluon distribution (also called unintegrated gluon distribution) function has been applied to describe various high energy hadronic processes [9].

In general, the initial and final state interaction effects associated with the transverse momentum dependent parton distributions introduce additional QCD dynamics in these processes. For example, they lead to the non-universality for the transverse spin dependent TMD parton distributions [4–6, 10–15]. In ref. [16], we extended the universality discussions of TMD parton distributions to the small- x domain. In order to study the factorization issues relevant to small- x saturation physics, it is of advantage to focus on the two scale processes, such as semi-inclusive hadron production in deep inelastic scattering, Drell-Yan lepton pair production in hadronic reactions, and the di-jet correlations in these processes. In particular, we analyzed the small- x transverse momentum dependent quark distributions probed in hadronic dijet-correlation in nucleon-nucleus collisions, as compared to that in the deep elastic lepton-nucleus (nucleon) scattering. Due to the nuclear enhancement, any soft gluon exchanges originated from the proton can be neglected. Thus, we only need to resum the soft gluon exchanges with the nucleus target in the large nuclear number limit. This procedure eventually helps us to obtain an effective k_t factorization with the modified nuclear parton distributions in pA collisions. There have been interesting experimental results on

di-hadron correlation in deuteron-gold collisions at RHIC, where a strong back-to-back de-correlation was found in the forward rapidity region of the deuteron as compared to the narrow back-to-back peaks observed in the central rapidity region [17]. The purposes of this paper are to derive in details the QED results which we described in ref. [16] where we have shown the non-universality of TMD parton distributions, and then generalize to small- x models in QCD.

We will start with a scalar-QED model calculation. There are a number of motivations for doing this. First, QED model is calculable, which makes it straightforward to resum all order initial and final state interaction effects in various processes. This allows us to rigorously discuss these effects, and shed light on the real QCD calculations. Second, there is similarity between the QED model calculations and the QCD saturation models. Quite a few results in the former framework can be directly generalized to the latter one. Third, the QED calculations are important in their own perspective. High order corrections in QED processes are interesting topics and have attracted intensive investigations since the QED was founded several decades ago. In particular, for the lepton pair production and photon radiation processes associated with large nucleus, higher order QED corrections have generated interests from both theory and experiment sides [18]. Current running heavy ion collisions experiments are pursuing these studies at both RHIC and LHC facilities. The theoretical investigations shall provide further understanding of these processes.

In the saturation domain of QCD, the McLerran-Venugopalan model [19] describes high density small- x partons in a relativistic large nucleus by treating the nucleus as a set of randomly distributed color sources $\rho_a(z^-, z_\perp)$ which generate soft classical gluon fields. Using the McLerran-Venugopalan model, we will demonstrate that the k_t dependent quark distributions at small- x are not universal and the quark distributions involved in DIS and di-jet production processes are distinct. Furthermore, we find a simple formula to relate these two quark distributions through a convolution with the normalized unintegrated gluon distribution.

The rest of the paper is organized as follows. In Sec. II, we construct a scalar QED model to investigate the universality property for the small- x parton distributions in various processes, where all gauge boson exchange contributions can be summed up, including all initial and final state interactions. In Sec. III, we demonstrate that the small- x TMD quark distributions of a large nucleus are not universal as well. In Sec. IV, we summarize our results.

II. INITIAL/FINAL STATE INTERACTIONS IN QED MODELS

In this section, we discuss the universality issue for the transverse momentum dependent parton distributions, by studying a scalar QED model. We will first introduce the QED model for our calculations, and discuss the universality issue of the TMD parton distribution functions in several processes.

A. Model Description

We follow Ref. [8] to construct the model for our calculations. This is a QED scalar model. It consists of heavy D and light ϕ charged scalars with masses M and m , respectively,

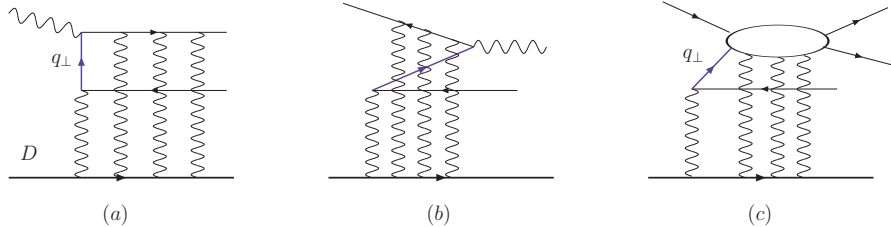


FIG. 1. Illustration of the final state interaction effects in DIS process (a), initial state interactions in Drell-Yan process (b), and initial/final state interactions in dijet-correlation process (c). In the dijet-correlation process, the gauge boson shall couple to any of the initial/final quarks.

interacting with massive U(1) gauge fields A_μ with the mass λ ,

$$\mathcal{L}_{\text{sQED}} = (\mathcal{D}_\mu \phi_1)^\dagger \mathcal{D}_\mu \phi_1 + (\mathcal{D}_\mu \phi_2)^\dagger \mathcal{D}_\mu \phi_2 + (\mathcal{D}_\mu D)^\dagger \mathcal{D}_\mu D - m^2 \phi^\dagger \phi - M^2 D^\dagger D - \frac{1}{4} F_{\mu\nu}^2 + \frac{\lambda^2}{2} A_\mu^2, \quad (1)$$

via the covariant derivative $\mathcal{D}_\mu \equiv \partial_\mu + igA_\mu$. In the above equation, we introduced two charged scalar particles, ϕ_1 and ϕ_2 with charges g_1 and g_2 , respectively. The purpose for this choice is to study the universality of the parton distribution in dijet-correlation.

We will adopt this model to calculate the DIS, Drell-Yan, and dijet processes. In particular, we will study the associated quark distribution functions in the small- x limit and investigate the universality issue. In Fig. 1, we plot the schematic diagrams for these processes in the scalar-QED model: (a) for DIS; (b) for Drell-Yan; (c) for dijet-correlation. In the DIS process (Fig. 1(a)), virtual photon scatters on the scalar quark from the nucleus target. In our example, the nucleus target has strong coupling with the Abelian gluon, $g \gg 1$. We need to resum all order gluon exchange contributions with the nucleus target, for which we have shown in the diagram. These interactions are referred as final state interactions. Similarly, we have multi-gluon interaction contribution between the incoming scalar quark with the nucleus target in the Drell-Yan process as shown in Fig. 1(b). For the dijet-correlation process in Fig. 1(c), there are both initial and final state interaction contributions.

The quark distribution functions in the DIS and Drell-Yan processes in this scalar-QED model have been calculated in the literature. Let us recapture the main step in these calculations. In the high energy scattering process, we apply the power counting method to separate short distance physics from that from long distance. This effectively factorizes the cross section in terms of parton distributions. In the multi-gluon exchange contributions illustrated in Fig. 1, the dominant contribution in high energy limit comes from the parton distribution in nucleus target. For example, in the DIS process, the leading power contribution to the differential cross section can be factorized into the quark distribution from nucleus in Fig. 1(a). Of course, higher order corrections will be taken into account for the gluon radiation diagrams.

The first step for this factorization is the eikonal approximation, which is valid in the leading power contribution, i.e., $1/Q^2$ for DIS and Drell-Yan processes. Under this limit, the final state interaction contribution diagram can be simplified as the eikonal propagator, which can also be summarized as the gauge link contribution from the associated parton distribution definition in these two processes. For the dijet-correlation, since there is no simple definition, we will not seek the gauge link definition for that, although there has been

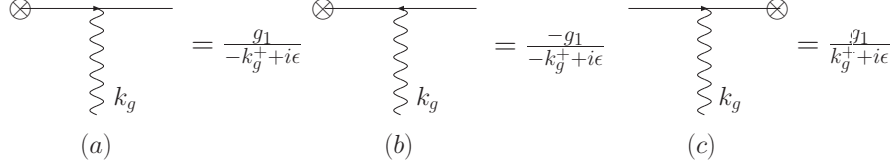


FIG. 2. Eikonal propagators for the initial/final state interactions in the scalar-QED model: (a) final state interaction on the scalar quark line; (b) final state interaction on the scalar antiquark line; (c) initial state interaction on scalar quark line.

attempt to do that in the literature[11]. However, we emphasize in the leading power contribution, we shall be able to obtain the effective parton distributions in terms of the parton transverse momentum and longitudinal momentum fraction. We notice that higher order corrections will introduce large logarithms. To correctly resum these large logarithms, we need to pay special attention to the transverse momentum dependent parton distributions. At the current level of this paper, we do not need to worry about this additional effect.

In the scalar-QED model, the eikonal approximation leads to the final state interaction effect in Fig. 2(a) as,

$$\frac{i}{(k - k_g)^2 - m^2 + i\epsilon} (-ig_1)(2k - k_g) \cdot P_A \approx \frac{g_1 P_A^+}{-k_g^+ + i\epsilon}, \quad (2)$$

which is the same as that for the fermionic propagator. Similarly, we will obtain the eikonal propagator for the final state interaction on the scalar antiquark as illustrated in Fig. 2(b), and the initial state interaction on the scalar quark in Fig. 2(c). The initial state interaction on the scalar antiquark will be opposite to that in Fig. 2(c). For the charge g_2 scalar quarks, we will have the same expressions by replacing g_1 with g_2 in these diagrams, respectively. In the following calculations, we will utilize these eikonal approximation for the relevant Feynman diagrams.

B. Universality of Quark Distributions Between SIDIS and Drell-Yan Processes

In this subsection, we review the known results[6, 8, 20] for the quark distributions in the above described model for the DIS and Drell-Yan lepton pair production processes in the small- x limit. In particular, we will perform the eikonal approximation on the final state interactions on the quark line. For the antiquark line with momentum p_2 , because its phase space is integrated out, we will keep the full kinematic dependence in these diagrams. The scalar quark (with charge g_1) distribution in DIS process can be written as

$$\tilde{q}^{\text{DIS}}(x, q_\perp) = \frac{x}{32\pi^2} \int \frac{dp_2^-}{p_2^-} \int \frac{d^2 k_\perp}{(2\pi)^4} |4P^+ p_2^- \sum_{n=1}^{\infty} (gg_1)^n A_N^{(n)}(k_\perp, k_\perp - q_\perp)|^2, \quad (3)$$

where the first three expansions of the amplitude are found as follows

$$A_{\text{DIS}}^{(1)} = \frac{1}{k_{\perp}^2 + \lambda^2} \left[\frac{1}{D_1} - \frac{1}{D_2} \right], \quad (4)$$

$$A_{\text{DIS}}^{(2)} = \frac{i}{2!} \int d[1]d[2] \left[\frac{1}{D_1} + \frac{1}{D_2} - \frac{2}{D_{12}} \right], \quad (5)$$

$$A_{\text{DIS}}^{(3)} = \frac{1}{3!} \int d[1]d[2]d[3] \left[-\frac{1}{D_1} + \frac{1}{D_2} - \frac{3}{D_{21}} + \frac{3}{D_{12}} \right]. \quad (6)$$

For convenience, we have defined the following integral,

$$\begin{aligned} \int d[1]d[2] &= \int \frac{d^2 k_{1\perp} d^2 k_{2\perp}}{(2\pi)^4} \frac{1}{k_{1\perp}^2 + \lambda^2} \frac{1}{k_{2\perp}^2 + \lambda^2} (2\pi)^2 \delta^{(2)}(k_{\perp} - k_{1\perp} - k_{2\perp}), \\ \int d[1]d[2]d[3] &= \int \frac{d^2 k_{1\perp} d^2 k_{2\perp} d^2 k_{3\perp}}{(2\pi)^6} \frac{1}{k_{1\perp}^2 + \lambda^2} \frac{1}{k_{2\perp}^2 + \lambda^2} \frac{1}{k_{3\perp}^2 + \lambda^2} \\ &\quad \times (2\pi)^2 \delta^{(2)}(k_{\perp} - k_{1\perp} - k_{2\perp} - k_{3\perp}). \end{aligned} \quad (7)$$

We have also defined $D(p_{\perp}) = 2xP^+p_2^- + p_{2\perp}^2 + m^2$, $D_1 = D(q_{\perp})$, $D_2 = D(p_{2\perp})$, $D_{1i} = D(q_{\perp} - k_{i\perp})$ and $D_{2i} = D(p_{2\perp} - k_{i\perp})$. To perform the resummation, we introduce the following Fourier transform,

$$\tilde{A}(R_{\perp}, r_{\perp}) = \int \frac{d^2 p_{2\perp}}{(2\pi)^2} \frac{d^2 k_{\perp}}{(2\pi)^2} A(k_{\perp}, p_{2\perp}) e^{-ik_{\perp} \cdot R_{\perp} - i\vec{p}_{2\perp} \cdot \vec{r}_{\perp}}. \quad (8)$$

By applying this Fourier transform, we obtain,

$$\tilde{A}_{\text{DIS}}^{(1)} = -V(r_{\perp})W(r_{\perp}, R_{\perp}), \quad (9)$$

$$\tilde{A}_{\text{DIS}}^{(2)} = +\frac{i}{2!} V(r_{\perp})W^2(r_{\perp}, R_{\perp}), \quad (10)$$

$$\tilde{A}_{\text{DIS}}^{(3)} = +\frac{1}{3!} V(r_{\perp})W^3(r_{\perp}, R_{\perp}), \quad (11)$$

where the functions V and W are defined as

$$V(r_{\perp}) = \frac{1}{2\pi} K_0(M_0 r_{\perp}), \quad (12)$$

$$W(r_{\perp}, R_{\perp}) = \frac{1}{2\pi} \log \left(\frac{|\vec{R}_{\perp} + \vec{r}_{\perp}|}{R_{\perp}} \right), \quad (13)$$

with $M_0^2 = 2xP^+p_2^- + m^2$, and K_0 is the Bessel function. Clearly, we can see that the above expansion comes from the following exponential form,

$$\tilde{A}_{\text{DIS}} = iV(r_{\perp}) [1 - e^{-igg_1 W(r_{\perp}, R_{\perp})}]. \quad (14)$$

Substituting the above result into the quark distribution expression, we will obtain the TMD quark distribution in the DIS process,

$$\begin{aligned} \tilde{q}^{\text{DIS}}(x, q_{\perp}) &= \frac{xP^{+2}}{8\pi^4} \int dp_2^- p_2^- \int d^2 R_{\perp} d^2 r_{\perp} d^2 r'_{\perp} e^{-i\vec{q}_{\perp} \cdot (\vec{r}_{\perp} - \vec{r}'_{\perp})} V(r_{\perp}) V(r'_{\perp}) \\ &\quad \times [1 - e^{-igg_1 W(r_{\perp}, R_{\perp})}] [1 - e^{-igg_1 W(r'_{\perp}, R_{\perp})}]. \end{aligned} \quad (15)$$

In Sec.III, we will discuss how to translate this result into the fermion quark distribution function at small- x for this process in QCD and compare to the color-dipole/color glass condensate formalism.

Similarly, one can calculate the quark distribution[20] in the Drell-Yan lepton pair production process. The definition of the quark distribution has the same expression as in Eq. (3). The amplitudes of first three orders are found to be

$$A_{\text{DY}}^{(1)} = \frac{1}{k_{\perp}^2 + \lambda^2} \left[\frac{1}{D_1} - \frac{1}{D_2} \right] , \quad (16)$$

$$A_{\text{DY}}^{(2)} = \frac{i}{2!} \left[\frac{1}{D_1} - \frac{1}{D_2} \right] \int d[1]d[2] , \quad (17)$$

$$A_{\text{DY}}^{(3)} = \frac{-1}{3!} \left[\frac{1}{D_1} - \frac{1}{D_2} \right] \int d[1]d[2]d[3] . \quad (18)$$

It is easier to do the resummation when we perform the Fourier transform, for which we have

$$\tilde{A}_{\text{DY}}^{(1)} = -V(r_{\perp}) \left[G(R_{\perp}) - G(\vec{R}_{\perp} + \vec{r}_{\perp}) \right] , \quad (19)$$

$$\tilde{A}_{\text{DY}}^{(2)} = -\frac{i}{2!} V(r_{\perp}) \left[G^2(R_{\perp}) - G^2(\vec{R}_{\perp} + \vec{r}_{\perp}) \right] , \quad (20)$$

$$\tilde{A}_{\text{DY}}^{(3)} = +\frac{1}{3!} V(r_{\perp}) \left[G^3(R_{\perp}) - G^3(\vec{R}_{\perp} + \vec{r}_{\perp}) \right] , \quad (21)$$

where $G(R_{\perp}) = \frac{1}{2\pi} K_0(\lambda R_{\perp})$. The all order resummation leads to

$$\tilde{A}_{\text{DY}} = iV(r_{\perp}) e^{igg_1 G(R_{\perp})} \left[1 - e^{igg_1 (G(\vec{R}_{\perp} + \vec{r}_{\perp}) - G(R_{\perp}))} \right] . \quad (22)$$

There is infrared divergence when the gluon mass goes to zero $\lambda \rightarrow 0$. However, this infrared divergence cancels out when we calculate the quark distribution. Furthermore, taking the limit $\lambda \rightarrow 0$, we also have $-G(\vec{R}_{\perp} + \vec{r}_{\perp}) + G(R_{\perp}) \rightarrow W(r_{\perp}, R_{\perp})$, and we can find that the quark distribution is universal between DIS and Drell-Yan processes

$$\tilde{q}^{\text{DY}}(x, q_{\perp}) = \tilde{q}^{\text{DIS}}(x, q_{\perp}) . \quad (23)$$

This universality is also guaranteed by the time-reversal invariance. The quark distributions in these two processes can be connected through time-reversal transformation, and time-reversal invariance can show that they are the same. However, this will not be the case when we compare the photon-jet correlation in Drell-Yan type process and dijet-correlation in DIS type process. We will carry out these calculations in future studies.

C. Non-universality of Quark Distribution Between Dijet-Correlation and SIDIS/DY Processes

To study the TMD scalar quark distribution in hadronic processes (e.g., pA collisions), we introduce the dijet-correlation process as illustrated in Fig. 1(c),

$$p + A \rightarrow \text{Jet1} + \text{Jet2} + X , \quad (24)$$

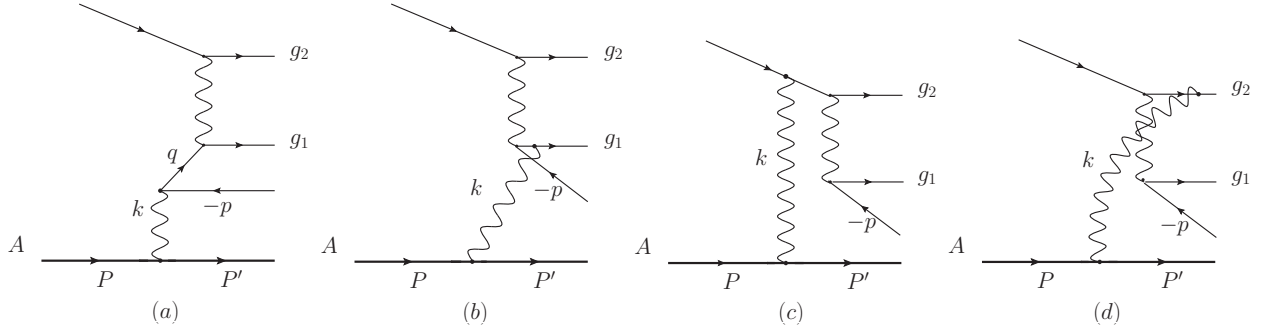


FIG. 3. Lowest-order graphs for di-jet production in a hadron-hadron collision in the small- x limit. In these graphs, there is one soft gluon exchange with momentum k in addition to the hard gluon exchange.

where the transverse momenta of these two jets are similar in size but opposite to each other in direction. For simplicity, we focus on the partonic channel $qq' \rightarrow qq'$ for now in this paper and study the quark distribution. We expect that similar conclusions can be drawn as to other partonic channels and thus to the gluon distributions as well. In the ideal case, these two jets are produced back-to-back. However, the gluon radiation and intrinsic transverse momenta of the initial partons induce an imbalance between them. We are particularly interested in the kinematic region that the imbalance $\vec{q}_\perp = \vec{P}_{1\perp} + \vec{P}_{2\perp}$ is much smaller than the transverse momentum of the individual jet, namely, $|\vec{q}_\perp| \ll |\vec{P}_{1\perp}| \sim |\vec{P}_{2\perp}|$, which also corresponds to the kinematics in the STAR measurements. Only in this region, can the intrinsic transverse momentum have significant effects. Since there are two incoming partons, both intrinsic transverse momenta can affect the imbalance between the two jets. For large nucleus and small- x , the dominant contribution should come from the intrinsic transverse momentum of the parton from the nucleus, which we label as q_\perp in Fig. 1(a). In the following, we will focus on this contribution.

Since we are interested in studying the final state interaction effects on the parton distribution of the nucleus, for convenience, we choose the projectile as a single scalar quark with charge g_2 , which differs from the charge of the scalar quark from the target nucleus, g_1 . In addition, we assume that the Abelian gluon attaches to the target nucleus with an effective coupling g which is much larger than g_2 or g_1 . All the partons in this calculation are set to be scalars with a mass m . The coupling g_2 being different from g_1 is to show the dependence of the parton distribution on the initial/final state interactions associated with the incoming parton. If the dependence on g_2 remains for the nucleus parton distributions, they are not universal [13, 14].

In Fig. 3, we plot the lowest-order graphs containing one soft gluon exchange with the momentum k . Following the discussions above, we keep the low transverse momentum approximation in terms of $q_\perp/P_{1\perp}$ ($q_\perp/P_{2\perp}$) by applying the power counting method [12]. Again, the important simplification is the eikonal approximation, which replaces the gluon attachment to the initial and final state partons with the eikonal propagator and vertex. After taking the leading order contributions, we find that the q_\perp dependence of these diagrams can be cast into an effective quark distribution [12], which takes the following form,

$$\tilde{q}(x, q_\perp) = \frac{x}{32\pi^2} \int \frac{dp^-}{p^-} \frac{d^2k_\perp}{(2\pi)^4} (4P^+ p^-)^2 |A^{(tot)}(k, p)|^2, \quad (25)$$

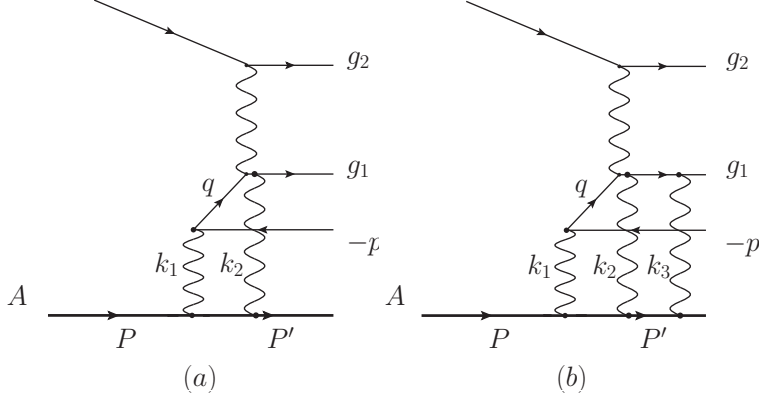


FIG. 4. Example diagrams for two (a) and three (b) gluons exchanges, where the gluons can attach all charged particles in the upper part of the diagrams to the nucleus target.

with $p_{\perp} = k_{\perp} - q_{\perp}$. Here, the hard partonic part depending on the hard momentum scale $P_{i\perp}$ has been separated from the above quark distribution in the differential cross section [12]. This separation is only possible at the leading power contribution of $q_{\perp}/P_{i\perp}$. The contributions from Fig. 2 can be written as,

$$A^{(1)}(k, p) = gg_1 \frac{1}{k_{\perp}^2 + \lambda^2} \left[\frac{1}{D_1} - \frac{1}{D_2} \right] + gg_2 \frac{1}{k_{\perp}^2 + \lambda^2} \frac{1}{2p^-} \left[\frac{1}{-k^+ + i\epsilon} + \frac{1}{k^+ + i\epsilon} \right], \quad (26)$$

where D_i follow the definitions introduced above. The first and second terms in the first square bracket correspond to Fig. 3 (a) and Fig. 3 (b), respectively. Fig. 3 (c) and Fig. 3 (d) yield the contributions as shown in the last term in Eq. (26). It is not hard to see that these two contributions simply cancel since the sum is proportional to $2\pi i\delta(k^+)$ while $k^+ \neq 0$. This means that at the leading order in the coupling constant the dependence on g_2 drops out, which will however change at higher orders. Thus, one gets $A^{(1)}(k, p) = gg_1 \frac{1}{k_{\perp}^2 + \lambda^2} \left[\frac{1}{D_1} - \frac{1}{D_2} \right]$.

At the next-to-leading order and the g^3 order, there are 20 and 120 graphs in total in covariant gauge, respectively. We show one of these graphs as an example in Fig. (4) (a) and (b), respectively. Additional diagrams can be obtained by attaching the gluons to all incoming and outgoing scalar quarks. We organize our calculations according to these attachments. Again, the eikonal approximation discussed at the beginning of this sections will be utilized in the evaluations of these diagrams. For example, by applying this approximation, we replace the final state QED-gluon interactions with the scalar quark line with the eikonal propagators and vertices associated with g_1 coupling, which we label with n_1 in Fig. 5. Similar approximations are made for all other diagrams, with n_2 and n_3 representing final and initial state QED-gluon interaction with the scalar quark line with charge g_2 . We summarize those diagrams in Fig. (5), where every graph except for (e) and (f) represents 3 graphs and total of 20 graphs contribute.

Among those 20 graphs, only a few sets of graphs give non-vanishing contributions. To better explain the calculation, let us first evaluate Fig. (5) (a) and (b) as an example.

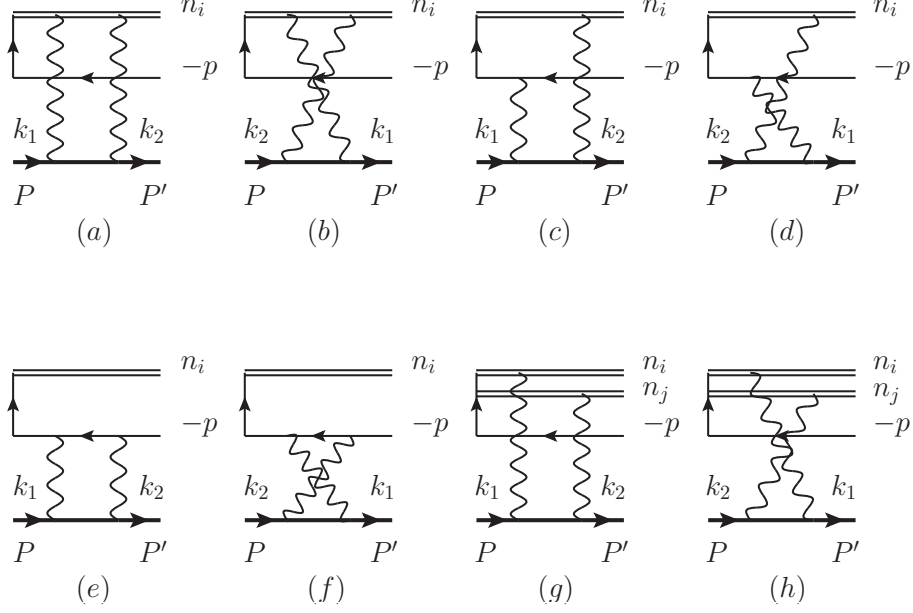


FIG. 5. Two-gluon-exchange contributions to the quark distribution. $i = 1, 2, 3$ for each n_i in each graph with $n_1 = \frac{g_1}{-k^+ + i\epsilon}$, $n_2 = \frac{g_2}{-k^+ + i\epsilon}$ and $n_3 = \frac{g_2}{k^+ + i\epsilon}$. $i \neq j$ for $n_{i,j}$ is implied in graphs (g) and (h).

Fig. (5)(a) and Fig. (5)(b) with $n_i = n_1$ give the following contribution

$$A_{a+b}^{(2,i=1)} = \frac{ig^2 g_1^2 (2P^+)^2}{4P^+ p^-} \int \frac{d^4 k_2}{(2\pi)^4} \frac{1}{k_1^2 - \lambda^2} \frac{1}{k_2^2 - \lambda^2} \frac{1}{k_2^+ - i\epsilon} \frac{1}{k^+ - i\epsilon} \times \left[\frac{1}{(P - k_1)^2 - m^2 + i\epsilon} + \frac{1}{(P - k_2)^2 - m^2 + i\epsilon} \right]. \quad (27)$$

After integrating over dk_2^- and dk_2^+ , one finds that the subtotal contribution reads

$$A_{a+b}^{(2,i)} = \frac{ig^2 g_1^2}{2} \int \frac{d^2 k_{2\perp}}{(2\pi)^2} \frac{1}{k_{1\perp}^2 + \lambda^2} \frac{1}{k_{2\perp}^2 + \lambda^2} \frac{1}{D(p_\perp)}. \quad (28)$$

It is straightforward to find that the contributions from n_2 and n_3 cancels and g_2^2 contribution vanishes due to the same reason we explained under Eq. (26).

As to the graphs illustrated in Fig. (5)(c) and Fig. (5)(d), we find that the contribution from n_3 vanishes due to vanishing contour integral of dk_2^+ . Thus, the subtotal contribution of Fig. (5)(c) and Fig. (5)(d) is

$$A_{c+d}^{(2,i)} = \frac{ig^2 (g_1^2 + g_1 g_2) (2P^+)^2 (-2p^-)}{4P^+ p^-} \int \frac{d^4 k_2}{(2\pi)^4} \frac{1}{k_1^2 - \lambda^2} \frac{1}{k_2^2 - \lambda^2} \frac{1}{k_2^+ - i\epsilon} \times \frac{1}{(p - k_1)^2 - m^2 + i\epsilon} \left[\frac{1}{(P - k_1)^2 - m^2 + i\epsilon} + \frac{1}{(P - k_2)^2 - m^2 + i\epsilon} \right], \quad (29)$$

with $k = k_1 + k_2$. After integrating over dk_2^- and dk_2^+ , one finds

$$A_{c+d}^{(2,i)} = -\frac{ig^2 (g_1^2 + g_1 g_2)}{2} \int \frac{d^2 k_{2\perp}}{(2\pi)^2} \frac{1}{k_{1\perp}^2 + \lambda^2} \frac{1}{k_{2\perp}^2 + \lambda^2} \left[\frac{1}{D(p_\perp - k_{1\perp})} + \frac{1}{D(p_\perp - k_{2\perp})} \right]. \quad (30)$$

Similarly, we obtain

$$A_{e+f}^{(2,i)} = -\frac{ig^2g_1^2}{2} \int \frac{d^2k_{2\perp}}{(2\pi)^2} \frac{1}{k_{1\perp}^2 + \lambda^2} \frac{1}{k_{2\perp}^2 + \lambda^2} \frac{1}{D(q_\perp)}, \quad (31)$$

and

$$A_{g+h}^{(2,i)} = ig^2g_1g_2 \int \frac{d^2k_{2\perp}}{(2\pi)^2} \frac{1}{k_{1\perp}^2 + \lambda^2} \frac{1}{k_{2\perp}^2 + \lambda^2} \frac{1}{D(p_\perp)}. \quad (32)$$

The total contributions are

$$A^{(2)}(k, p) = \frac{i}{2}g^2 \int d[1]d[2] \left\{ g_1^2 \left[\frac{1}{D_1} + \frac{1}{D_2} - \frac{1}{D_{21}} - \frac{1}{D_{22}} \right] + g_1g_2 \left[\frac{2}{D_2} - \frac{2}{D_{21}} \right] \right\}, \quad (33)$$

where $\int d[1]d[2]$ stands for the same definition as in Eq. (7), $D_{1i} = D(q_\perp - k_{i\perp})$ and $D_{2i} = D(p_\perp - k_{i\perp})$. Clearly, the second order result shows a dependence on g_2 . However, in the amplitude squared calculation for the quark distribution Eq. (25), the g_2 dependence from $A^{(1)}A^{(2)*}$ is canceled out by its complex conjugate because $A^{(1)}$ is real while $A^{(2)}$ is purely imaginary. The leading order contribution to g_2 comes from $|A^{(2)}(k, p)|^2$ and $A^{(1)}A^{(3)*} + A^{(3)}A^{(1)*}$. Therefore, to see the residue dependence on g_2 , we need to carry out the calculation of the amplitude up to order g^3 .

At the g^3 order, there are 120 diagrams in total with three soft gluon-exchange (see e.g., Fig. 4 (b)), including all possible permutations of the attachments of these three gluons to the target nucleus. Let us take Fig. 4 (b) as an example together with the other 5 crossing diagrams. The corresponding contribution is

$$I_1^{(3)} = -\frac{g^3g_1^3}{2} \int \frac{d^2k_{1\perp}d^2k_{2\perp}}{(2\pi)^4} \frac{1}{k_{1\perp}^2 + \lambda^2} \frac{1}{k_{2\perp}^2 + \lambda^2} \frac{1}{k_{3\perp}^2 + \lambda^2} \frac{1}{D(p_\perp - k_{1\perp})}. \quad (34)$$

In reaching above result, we have used the following two integrals:

$$\begin{aligned} & \int \frac{dk_1^- dk_2^- dk_3^-}{(2\pi)^2} \delta(k^- - k_1^- - k_2^- - k_3^-) \\ & \times \left[\frac{i}{(P - k_1)^2 - m^2 + i\epsilon} \frac{i}{(P - k_1 - k_2)^2 - m^2 + i\epsilon} + \text{Crossing Diagrams} \right] \\ & = \frac{-1}{4P^{+2}} \int \frac{dk_2^- dk_3^-}{(2\pi)^2} \frac{k^-}{(k^- - k_2^- - k_3^- - i\epsilon)(k_2^- - i\epsilon)(k_3^- - i\epsilon)} = \frac{1}{4P^{+2}}. \end{aligned} \quad (35)$$

and

$$\begin{aligned} & \int \frac{dk_1^+ dk_2^+ dk_3^+}{(2\pi)^2} \delta(k^+ - k_1^+ - k_2^+ - k_3^+) \\ & \times \left[\frac{i}{(p - k_1)^2 - m^2 + i\epsilon} \frac{i}{-k_3^+ + i\epsilon} \frac{i}{-k_2^+ - k_3^+ + i\epsilon} \right] \\ & = -\frac{i}{2} \frac{1}{D(p_\perp - k_{1\perp})}. \end{aligned} \quad (36)$$

Summing up all these graphs, we obtain the three gluon exchange amplitude,

$$A^{(3)}(k, p) = \frac{1}{3!} g^3 \int d[1]d[2]d[3] \left\{ g_1^3 \left[\frac{1}{D_2} - \frac{1}{D_1} + \frac{3}{D_{13}} - \frac{3}{D_{21}} \right] + g_1^2 g_2 \left[\frac{3}{D_2} + \frac{3}{D_{13}} - \frac{3}{D_{21}} - \frac{3}{D_{22}} \right] + g_1 g_2^2 \left[\frac{3}{D_2} - \frac{3}{D_{21}} \right] \right\}, \quad (37)$$

where $\int d[1]d[2]d[3]$ follows the same definition as in Eq. (7). Again, we see the dependence on g_2 in the second and third terms. An important cross check of these results is that, if we set $g_2 = -g_1$, there is effectively no charge flow in the final state, and the quark distribution is identical to that in the Drell-Yan process in the same model. Applying $g_2 = -g_1$, we can easily see that indeed we reproduce those calculated in Ref. [20]. Also, by setting $g_2 = 0$, we can recover the DIS amplitudes.

With the amplitude calculated up to $\mathcal{O}(g^3)$, we are able to check the dependence on g_2 for the parton distribution in Eq. (25). Substituting the above amplitudes into Eq. (25), we find that the g_2 dependence still remains up to order g^4 . If we drop all g_2 terms in these results, we obtain the quark distribution in DIS in the same model [6, 8]. This clearly shows that the TMD quark distribution $\tilde{q}(x, q_\perp)$ is not universal.

This non-universality is better illustrated when we sum up all order multi-gluon exchange contributions. To do that, we introduce the following Fourier transform [8],

$$A(R, r) = \int \frac{d^2 k_\perp}{(2\pi)^2} \frac{d^2 p_\perp}{(2\pi)^2} e^{-ik_\perp \cdot R_\perp - ip_\perp \cdot r_\perp} A(k, p). \quad (38)$$

From the Fourier transforms of $A^{(1,2,3)}(k, p)$, we can easily see that they follow the expansion of an exponential form,

$$A^{(tot)}(R, r) = \sum_{n=1}^{\infty} A^{(n)}(R, r) = iV(r_\perp) \left\{ 1 - e^{igg_1[G(R_\perp + r_\perp) - G(R_\perp)]} \right\} e^{-igg_2 G(R_\perp)}, \quad (39)$$

where $G(R_\perp) = K_0(\lambda R_\perp)/2\pi$ and $V(r_\perp) = K_0(Mr_\perp)/2\pi$ with $M^2 = 2xP^+p^- + m^2$. In the above result, the g_2 -dependence seems to only appear as a phase which may not lead to a physics consequence. However, because the transverse momentum q_\perp is conjugate to the coordinate variable difference $R_\perp - r_\perp$, this phase will lead to a non-universal contribution to the quark distribution as defined in Eq. (25). Here we can identify the factor $e^{-igg_2 G(R_\perp)}$ as a Wilson line which essentially resums soft interactions between quarks and the target nucleus.

Therefore, the all order result reads,

$$\begin{aligned} \tilde{q}(x, q_\perp) &= \frac{xP^+2}{8\pi^4} \int dp^- p^- \int d^2 R_\perp d^2 R'_\perp d^2 r_\perp d^2 r'_\perp \delta^{(2)}(R_\perp + r_\perp - R'_\perp - r'_\perp) \\ &\quad \times e^{-iq_\perp \cdot (r_\perp - r'_\perp)} e^{-igg_2(G(R_\perp) - G(R'_\perp))} V(r_\perp) V(r'_\perp) \\ &\quad \times \left\{ 1 - e^{igg_1[G(R_\perp + r_\perp) - G(R_\perp)]} \right\} \left\{ 1 - e^{-igg_1[G(R'_\perp + r'_\perp) - G(R'_\perp)]} \right\}, \end{aligned} \quad (40)$$

This TMD quark distribution is clearly different from that calculated in DIS in the same model [6, 8]. In other words, TMD quark distributions are not universal. It is interesting to notice that the g_2 dependence disappears after the integration over the transverse

momentum. This is consistent with the universality for the integrated parton distributions [6, 13, 14]. In spite of the non-universality, we expect that one can still reach an effective TMD factorization formula for pA collisions by absorbing all the violation effects into the parton distributions as in Eq. (40).

It has been argued that the light-cone gauge may simplify the factorization property for the hard scattering processes. For example, if we choose the advanced boundary condition for the gauge potential in light-cone gauge, the wave function of hadrons contain the final state interaction effects [6, 21]. However, as we showed in the above calculations, this does not help to resolve the g_2 -dependence in the quark distribution in the dijet correlation in hadronic process due to the presence of both initial and final state interactions. In other words, the quark distribution from the nucleus target has to contain the interaction with the incoming (outgoing) quark with charge g_2 , which can not be solely included into the wave function of the nucleus target.

III. EXTENSION TO THE QUARK DISTRIBUTIONS AT SMALL- x IN CGC

In this section, we extend the previous calculation to the quark distribution functions for a large nucleus at small- x in QCD, by calculating the similar resummation effects due to initial and final state interactions. As an example, we follow the McLerran-Venugopalan (MV) Model [19]. The MV model describes high density gluon distribution in a relativistic large nucleus by solving the classical Yang-Mills equation. An effective theory, called the Color Glass Condensate (CGC), is developed to study the high density physics in QCD in a systematic manner [9]. It is equivalent to the saturation picture which is based on the color dipole model[22, 23] in terms of quantitatively describing the parton saturation at small- x . In our following discussion, we will focus on the CGC formalism since it is close to what we have used above in the QED model.

Following the CGC formalism, the target nucleus is treated as a collection of randomly distributed color sources $\rho_a(z^-, z_\perp)$ which generate soft classical gluon fields. Similar to what happens in above QED model, where we obtain the Wilson line $e^{-igg_i[G(x_\perp)]}$, the soft interactions (i.e., the soft gluon exchanges) between the nucleus and a relativistic quark can also be resummed into a Wilson line which reads

$$U(x_\perp) = T \exp \left[-igg_1 \int dz^- d^2 z_\perp G(x_\perp - z_\perp) \rho_a(z^-, z_\perp) t^a \right], \quad (41)$$

where t^a is the $SU(3)$ color matrix in the fundamental representation and the two-dimensional propagator $G(x_\perp - z_\perp)$ is the same as the one we used in the scalar QED model. The differences come from the fact that the target nucleus is no longer treated as point particles and quarks now carry colors. It is straightforward to see that we recover the scalar-QED model result ($U(x_\perp) \Rightarrow e^{-igg_1[G(x_\perp)]}$) if we apply the point particle approximation: $\rho_a(z^-, z_\perp) t^a \Rightarrow \delta(z^-) \delta^{(2)}(z_\perp)$. In addition, the ensemble average over the color sources should be performed. Since one assumes the color sources are randomly distributed, a Gaussian distribution $W[\rho]$ is always used in the average. In the McLerran-Venugopalan Model, the Gaussian distribution is defined as follows [9]

$$W[\rho] = \exp \left[- \int dz^- d^2 z_\perp \frac{\rho_a(z^-, z_\perp) \rho_a(z^-, z_\perp)}{2\mu^2(z^-)} \right]. \quad (42)$$

The variance $\mu^2(z^-)$ of the charge distribution represents the density of color sources per unit volume. It is assumed that the average in CGC is performed in a functional integration over ρ accompanied by $W[\rho]$. It then follows that

$$\begin{aligned} \langle \rho_a(x^-, x_\perp) \rho_b(y^-, y_\perp) \rangle_\rho &= \int \mathcal{D}\rho W[\rho] \rho_a(x^-, x_\perp) \rho_b(y^-, y_\perp) \\ &= \delta_{ab} \delta(x^- - y^-) \delta^{(2)}(x_\perp - y_\perp) \mu^2(x^-). \end{aligned} \quad (43)$$

This turns out to be useful in the following derivations for the TMD parton distributions in CGC.

A. DIS and Drell-Yan Processes

As we discuss in Sec.II, the TMD quark distribution in DIS in the scalar QED model can be written as

$$\begin{aligned} \tilde{q}^{\text{DIS}}(x, q_\perp) &= \frac{xP^{+2}}{8\pi^4} \int dp^- p^- \int d^2 R_\perp d^2 R'_\perp d^2 r_\perp d^2 r'_\perp \\ &\quad \times \delta^{(2)}(R_\perp + r_\perp - R'_\perp - r'_\perp) e^{iq_\perp \cdot (R_\perp - R'_\perp)} V(r_\perp) V(r'_\perp) \\ &\quad \times \left\{ 1 - e^{igg_1[G(R_\perp + r_\perp) - G(R_\perp)]} \right\} \left\{ 1 - e^{-igg_1[G(R'_\perp + r'_\perp) - G(R'_\perp)]} \right\}. \end{aligned} \quad (45)$$

To derive the above result, we have assumed the target hadron (nucleus) to be a point particle. In order to calculate the quark distribution in CGC, we need to relax the point particle approximation. Following the above discussions, we first assume that the target hadron has a color charge distribution $\rho_a(z^-, z_\perp)$ and perform a replacement $e^{-igg_1[G(x_\perp)]} \Rightarrow U(x_\perp)$.

The second step is to average over the color sources $\rho_a(z^-, z_\perp)$, which appears in the exponents of the Wilson lines $U(x_\perp)$, with the Gaussian distribution $W[\rho]$. Following this procedure, one finds (see Refs. [24–26])

$$\begin{aligned} e^{igg_1[G(R_\perp + r_\perp) - G(R_\perp)]} &\Rightarrow \text{Tr} \langle U^\dagger(R_\perp + r_\perp) U(R_\perp) \rangle_\rho \\ &= N_c \exp \left\{ -\mu_s^2 \int d^2 z_\perp [G(R_\perp + r_\perp - z_\perp) - G(R_\perp - z_\perp)]^2 \right\} \\ &= N_c \exp \left\{ -\mu_s^2 \int d^2 z_\perp [G(r_\perp + z_\perp) - G(z_\perp)]^2 \right\} \\ &\simeq N_c \exp \left\{ -Q_s^2 r_\perp^2 / 4 \right\}, \end{aligned} \quad (46)$$

where $N_c = 3$ is the number of colors, the saturation scale Q_s is defined as $Q_s^2 = \frac{\mu_s^2}{2\pi} \ln \frac{1}{r_\perp^2 \lambda^2}$ with $\mu_s^2 = \frac{g^2 g_1^2}{2} t^a t_a \int dx^- \mu^2(z^-)$. In the evaluation of the above two-point functions $\langle U^\dagger(R_\perp + r_\perp) U(R_\perp) \rangle_\rho$, we have assumed that the nucleus size is so large that we can shift R_\perp in the transverse integration. The saturation momentum naturally arises as a result of multiple scatterings between the hard parton and color charges inside the nucleus.

The next step is to use fermionic quark splitting kernel instead of the scalar quark splitting kernel. Thus we replace $V(r_\perp)$ in Eq. (45) by $\frac{1}{2\pi} 2K_1(Mr_\perp)$ where the factor of 2 comes from the fact that fermionic quark has two different helicities. It is straightforward to derive

this fermionic quark splitting kernel as in Ref. [27]. The rest of the calculation will remain the same since the eikonal propagator for a fermionic quark is the same as the one for a scalar quark as in Eq. (2). After changing the integral variable to $y = 2xP^+p^-$, we can cast the quark distribution into

$$x\tilde{q}^{\text{DIS}}(x, q_\perp) = \frac{N_c}{32\pi^6} \int dy d^2 R_\perp d^2 r_\perp d^2 r'_\perp e^{-iq_\perp \cdot (r_\perp - r'_\perp)} \nabla_{r_\perp} K_0(\sqrt{y}r_\perp) \cdot \nabla_{r'_\perp} K_0(\sqrt{y}r'_\perp) \\ \times \left\{ 1 + \exp\left[-\frac{Q_s^2(r_\perp - r'_\perp)^2}{4}\right] - \exp\left[-\frac{Q_s^2 r_\perp^2}{4}\right] - \exp\left[-\frac{Q_s^2 r'^2_\perp}{4}\right] \right\}. \quad (47)$$

The virtuality of the virtual photon $Q^2 = 2xP^+P^-$ is taken to be much larger than Q_s^2 and q_\perp^2 . Therefore, one can approximately integrate y from 0 to $+\infty$. The dominant contribution comes from the region where y is close to 0. It is hard to evaluate above integrals analytically. Nevertheless, we can study the quark distribution in the large and small q_\perp^2 limit, which give

$$\left. \frac{dx\tilde{q}^{\text{DIS}}(x, q_\perp)}{d^2 R_\perp} \right|_{q_\perp^2 \gg Q_s^2} = \frac{N_c}{12\pi^4} \frac{Q_s^2}{q_\perp^2} \\ \left. \frac{dx\tilde{q}^{\text{DIS}}(x, q_\perp)}{d^2 R_\perp} \right|_{q_\perp^2 \ll Q_s^2} = \frac{N_c}{4\pi^4}. \quad (48)$$

These results agree with those derived in the saturation model for the quark distribution of a large nucleus in DIS (see e.g., Eqs.(27-29) of Ref. [27])¹. Furthermore, we can transform the above results to the momentum space and define the normalized unintegrated gluon distribution $F(k_\perp, Q_s)$ as

$$F(k_\perp, Q_s) = \int \frac{d^2 r_\perp}{(2\pi)^2} e^{-ik_\perp \cdot r_\perp} \frac{\text{Tr}\langle U(R_\perp) U^\dagger(R_\perp + r_\perp) \rangle_\rho}{N_c} \simeq \frac{1}{\pi Q_s^2} \exp\left(-\frac{k_\perp^2}{Q_s^2}\right). \quad (49)$$

In arriving at the Gaussian form of $F(k_\perp, Q_s)$ in Eq. (49), we have neglected the logarithmic dependence of r_\perp^2 in the saturation momentum Q_s . Thus, one can write the quark distribution as a convolution of the unintegrated gluon distribution and the splitting kernel in momentum space,

$$x\tilde{q}^{\text{DIS}}(x, q_\perp) = \frac{N_c}{4\pi^4} \int d^2 R_\perp d^2 k_\perp F(q_\perp - k_\perp, Q_s) \int dy \left| \frac{\vec{q}_\perp}{q_\perp^2 + y} - \frac{\vec{k}_\perp}{k_\perp^2 + y} \right|^2 \\ = \frac{N_c}{4\pi^4} \int d^2 R_\perp d^2 k_\perp F(k_\perp, Q_s) \left[1 - \frac{q_\perp \cdot (q_\perp - k_\perp)}{q_\perp^2 - (q_\perp - k_\perp)^2} \ln \frac{q_\perp^2}{(q_\perp - k_\perp)^2} \right], \quad (50)$$

which is consistent with the results obtained in Ref. [28, 29]. The unintegrated gluon distribution $F(k_\perp, Q_s)$ is usually defined through the scattering amplitude of a dipole with size r_\perp on the target nucleus [30, 31]. This dipole scattering amplitude is also equivalent to the expectation value of a Wilson loop with width r_\perp and infinite length as we used above.

¹ We notice that there is a factor of 1/2 difference between our results and those obtained in Ref. [27]. This difference comes from the fact that the quark distribution calculated in Ref. [27] is in fact the total quark distribution which includes anti-quark distribution as well.

For comparison, we can also calculate the quark distribution involved in the Drell-Yan process. Again, we start with scalar-QED model result [20],

$$\begin{aligned} \tilde{q}^{\text{DY}}(x, q_\perp) = & \frac{xP^{+2}}{8\pi^4} \int dp^- p^- \int d^2 R_\perp d^2 R'_\perp d^2 r_\perp d^2 r'_\perp \\ & \times \delta^{(2)}(R_\perp + r_\perp - R'_\perp - r'_\perp) e^{iq_\perp \cdot (R_\perp - R'_\perp)} V(r_\perp) V(r'_\perp) \\ & \times \left\{ e^{igg_1 G(R_\perp + r_\perp)} - e^{igg_1 G(R_\perp)} \right\} \left\{ e^{-igg_1 G(R'_\perp + r'_\perp)} - e^{-igg_1 G(R'_\perp)} \right\}, \quad (51) \end{aligned}$$

Following the same procedures, we find that the quark distribution in the Drell-Yan process in the CGC formalism reads as

$$\begin{aligned} x\tilde{q}^{\text{DY}}(x, q_\perp) = & \frac{N_c}{32\pi^6} \int dy \int d^2 R_\perp d^2 r_\perp d^2 r'_\perp e^{-iq_\perp \cdot (r_\perp - r'_\perp)} \nabla_{r_\perp} K_0(\sqrt{y}r_\perp) \cdot \nabla_{r'_\perp} K_0(\sqrt{y}r'_\perp) \\ & \times \left\{ 1 + \exp\left[-Q_s^2(r_\perp - r'_\perp)^2/4\right] - \exp\left[-Q_s^2 r_\perp^2/4\right] - \exp\left[-Q_s^2 r'^2_\perp/4\right] \right\}. \quad (52) \end{aligned}$$

The quark distribution in the Drell-Yan process is the same as that in DIS, which is consistent with the conclusion in the scalar QED model, as the QCD factorization predicts.

B. Dijet production in pA Collisions

Finally, let us consider the TMD quark distribution for a large nucleus involved in the di-jet production, again, taking the $qq' \rightarrow qq'$ channel as an example. In the scalar-QED model, the TMD quark distribution in this process is shown in Eq. (40). In order to extend to the real QCD calculation, we will assume that the color charge for quark q' is the same as the quark q in the sense of the average over the large nucleus. This means that we will set $g_2 = g_1$ in the scalar-QED result². Furthermore, we find that the quark distribution here will naturally involve four-point function. For example, expanding the phase factor in Eq. (40) will depend on the four-point function in the CGC formalism,

$$\begin{aligned} e^{-igg_1(G(R_\perp) - G(R'_\perp))} \left\{ 1 - e^{igg_1[G(R_\perp + r_\perp) - G(R_\perp)]} \right\} \left\{ 1 - e^{-igg_1[G(R'_\perp + r'_\perp) - G(R'_\perp)]} \right\} \implies \\ \left\{ \begin{aligned} & U(R_\perp) U^\dagger(R'_\perp) + U(R_\perp) U^\dagger(R'_\perp) U(R_\perp) U^\dagger(R'_\perp) \\ & - U(R_\perp) U^\dagger(R'_\perp) U(R_\perp) U^\dagger(R_\perp + r_\perp) - U(R_\perp) U^\dagger(R'_\perp) U(R'_\perp + r'_\perp) U^\dagger(R'_\perp) \end{aligned} \right\} \quad (53) \end{aligned}$$

The appearance of the four point functions signals the difference between the di-jet production process and DIS, whereas the latter only involves two point functions. This indicates that parton distributions directly extracted from DIS are not sufficient to compute and describe the dijet production processes.

We can further simplify the above result by taking the large N_c limit for the four point functions [32]

$$\langle U(R_\perp) U^\dagger(R'_\perp) U(R_\perp) U^\dagger(R_\perp + r_\perp) \rangle_\rho \simeq \exp\left\{ -\frac{Q_s^2}{4} \left[(r_\perp - r'_\perp)^2 + r_\perp^2 \right] \right\}. \quad (54)$$

² This can be checked against the lowest nontrivial order perturbation expansion of the multi-gluon exchange contributions in the large N_c limit. As we mentioned before, setting $g_2 = -g_1$ will lead to the quark distribution in the Drell-Yan process.

With this reduction, we arrive at the following quark distribution in the large N_c limit,

$$x\tilde{q}^{\text{DJ}}(x, q_\perp) = \frac{N_c}{32\pi^6} \int dy d^2 R_\perp d^2 r_\perp d^2 r'_\perp e^{-iq_\perp \cdot (r_\perp - r'_\perp)} \nabla_{r_\perp} K_0(\sqrt{y} r_\perp) \cdot \nabla_{r'_\perp} K_0(\sqrt{y} r'_\perp) \\ \times \left\{ \begin{array}{l} \exp\left[-\frac{Q_s^2(r_\perp - r'_\perp)^2}{4}\right] + \exp\left[-\frac{Q_s^2(r_\perp - r'_\perp)^2}{2}\right] \\ - \exp\left[-\frac{Q_s^2((r_\perp - r'_\perp)^2 + r_\perp^2)}{4}\right] - \exp\left[-\frac{Q_s^2((r_\perp - r'_\perp)^2 + r'^2_\perp)}{4}\right] \end{array} \right\}, \quad (55)$$

which then yields

$$\left. \frac{dx\tilde{q}^{\text{DJ}}(x, q_\perp)}{d^2 R_\perp} \right|_{q_\perp^2 \gg Q_s^2} = \frac{N_c}{12\pi^4} \frac{Q_s^2}{q_\perp^2} \\ \left. \frac{dx\tilde{q}^{\text{DJ}}(x, q_\perp)}{d^2 R_\perp} \right|_{q_\perp^2 \ll Q_s^2} = 0.44 \frac{N_c}{4\pi^4}. \quad (56)$$

It is straightforward to see that the quark distributions in DIS and di-hadron production have the same perturbative tails while they differ in the small q_\perp^2 limit. As shown in Fig. 6, the quark distribution is about twice broader than the one in DIS while its peak is about half of the peak of the DIS distribution. However, it is easy to check analytically and numerically that the integrated quark distributions are universal for these processes.

In the momentum space, we find that the quark distribution in di-jet production can be written as follows:

$$x\tilde{q}^{\text{DJ}}(x, q_\perp) = \frac{N_c}{4\pi^4} \int d^2 R_\perp \int d^2 l_\perp F(q_\perp - l_\perp, Q_s) \\ \times \int d^2 k_\perp F(k_\perp, Q_s) \left[1 - \frac{l_\perp \cdot (l_\perp - k_\perp)}{l_\perp^2 - (l_\perp - k_\perp)^2} \ln \frac{l_\perp^2}{(l_\perp - k_\perp)^2} \right], \quad (57)$$

which implies that

$$x\tilde{q}^{\text{DJ}}(x, q_\perp) = \int d^2 l_\perp x\tilde{q}^{\text{DIS}}(x, l_\perp) F(q_\perp - l_\perp, Q_s). \quad (58)$$

This is an interesting new result. It relates the two apparently different quark distributions through a k_t convolution with the unintegrated gluon distribution $F(q_\perp - l_\perp, Q_s)$. It is easy to see that both quark distribution reduce to the same form after integration over q_\perp since $F(q_\perp - l_\perp, Q_s)$ is normalized to 1. In addition, Eq. (58) explains the broadening of the di-jet quark distribution as shown in Fig. 6. This formula has a natural physical interpretation. This convolution arises as a result of the extra initial and final state interactions in the di-jet production process.

IV. SUMMARY AND DISCUSSIONS

In this paper, we have studied the initial and final state interaction effects in the small- x parton distributions. As an example, we discussed the quark distributions in the semi-inclusive deep inelastic scattering, Drell-Yan lepton pair production and dijet-correlation in pA collisions. We calculated these distributions first in a scalar-QED model and then extended to the CGC formalism in QCD.

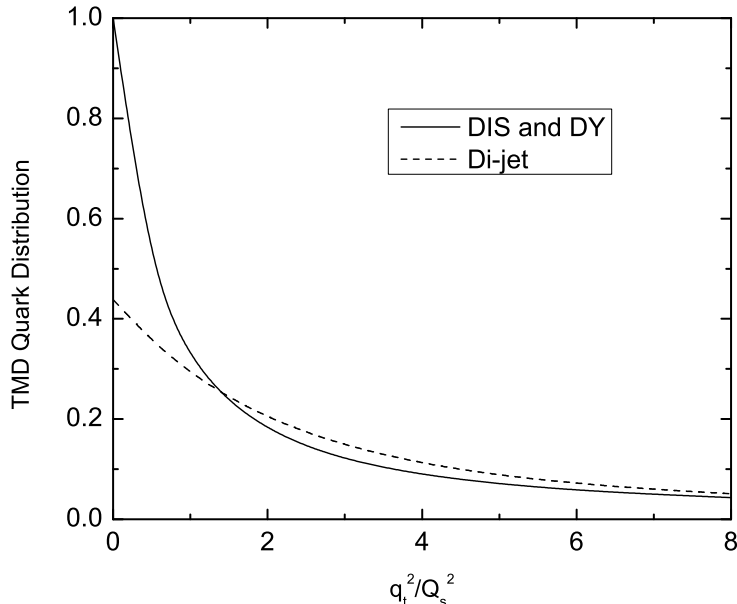


FIG. 6. Comparison of quark distributions $\frac{4\pi^4}{N_c} \frac{dx\tilde{q}(x, q_\perp)}{d^2R_\perp}$ as functions of $\frac{q_t^2}{Q_s^2}$ in DIS (or Drell-Yan) and di-hadron production. The solid curve stands for the quark distribution in DIS and Drell-Yan process, and the dash curve represents the distribution involved in di-hadron production.

We have shown the non-universality for the small- x parton distributions in dijet correlation in the scalar QED model calculations, as compared to the quark distributions in DIS and Drell-Yan processes. For the particular partonic channel $qq' \rightarrow qq'$, we find that the net effects are summarized into a phase which leads to a non-vanishing contribution to the quark distribution and breaks the universality.

We have also calculated the TMD quark distribution involved in dijet production in the saturation models [9, 27]. We reached the conclusion that TMD quark distributions are not universal in the color-dipole or color glass condensate formalism, by showing that the quark distributions involved in DIS and di-jet production processes are distinct as shown in Fig. 6. In addition, we found a simple formula which relates these two different quark distributions through a convolution with a normalized gluon distribution.

It is interesting to note that we can also compare to the quark distribution discussed in Refs. [11], where the initial and final state interaction effects are summed into an effective gauge link associated with the quark distribution. For example, for the partonic channel $qq' \rightarrow qq'$, the quark distribution requires the gauge link as $G = \frac{N_c^2+1}{N_c^2-1} \frac{\text{Tr}(\mathcal{U}^{[\square]})}{N_c} \mathcal{U}^{[+]} - \frac{2}{N_c^2-1} \mathcal{U}^{[\square]} \mathcal{U}^{[-]}$ which is different from that in the semi-inclusive DIS process with $G = \mathcal{U}^{[+]}$. In the large N_c limit, the additional gauge link structure would contribute a factor which is similar to the unintegrated gluon distribution in the CGC formalism as we have shown in Sec.III.

Despite the non-universality, we expect that there exists a generalized TMD factorization for the di-jet production in pA collisions in the large A limit. Thanks to the nuclear en-

hancement, which allows us to neglect any soft gluon exchanges originated from the proton, we can resum all the anomalous terms which breaks the k_t factorization and put them into the parton distributions of the target nucleus. This procedure leads to an effective k_t factorization with non-universal nuclear parton distributions in pA collisions. Also we would like to emphasize that the Wilson line $U(x_\perp)$, which provides the underlying fundamental description of the interactions between partons and dense hadronic matter, is still universal.

Of course in the high energy limit, the forward di-jet production in pA collisions is dominated by the $qg \rightarrow qg$ channel due to high gluon density in the target nucleus. This calculation is much more complicated than the $qq' \rightarrow qq'$ process which we considered in this paper. The complexity comes from the fact that there are many more channels involved in the $qg \rightarrow qg$ process. There have been some theoretical calculations[33, 34] in CGC. However, the non-universality issue has not yet been taken into consideration. We will address this problem together with the photon-jet productions in pA collisions in a future publication [35].

The non-universality for the TMD parton distributions at small- x clearly imposes a challenge in explaining the dijet-correlation data in dA collisions at RHIC with the parton distributions extracted *directly* from the DIS data. The non-universality, on the other hand, provides an opportunity to study QCD dynamics associated with the initial and final state interaction effects, which are calculable at small- x (high gluon density limit) according to our results. More phenomenological discussion will be provided in ref. [35].

V. ACKNOWLEDGMENT

We thank Tony Baltz, Stan Brodsky, Fabio Dominguez, Paul Hoyer, Cyrille Marquet, Larry McLarran, Al Mueller, Jianwei Qiu and Raju Venugopalan for interesting discussions. This work was supported in part by the U.S. Department of Energy under contracts DE-AC02-05CH11231. We are grateful to RIKEN, Brookhaven National Laboratory and the U.S. Department of Energy (contract number DE-AC02-98CH10886) for providing the facilities essential for the completion of this work.

-
- [1] J. C. Collins, D. E. Soper and G. Sterman, Adv. Ser. Direct. High Energy Phys. **5**, 1 (1988).
 - [2] K. Goeke, M.V. Polyakov, and M. Vanderhaeghen, Prog. Part. Nucl. Phys. **47**, 401 (2001); M. Diehl, Phys. Rep. **388**, 41 (2003); X. Ji, Ann. Rev. Nucl. Part. Sci. **54**, 413 (2004); A.V. Belitsky and A.V. Radyushkin, Phys. Rep. **418**, 1 (2005); S. Boffi and B. Pasquini, Riv. Nuovo Cim. **30**, 387 (2007).
 - [3] X. Ji, Phys. Rev. Lett. **91**, 062001 (2003); A. V. Belitsky, X. Ji and F. Yuan, Phys. Rev. D **69**, 074014 (2004).
 - [4] S. J. Brodsky, D. S. Hwang and I. Schmidt, Phys. Lett. B **530**, 99 (2002); Nucl. Phys. B **642**, 344 (2002).
 - [5] J. C. Collins, Phys. Lett. B **536**, 43 (2002).
 - [6] X. Ji and F. Yuan, Phys. Lett. B **543**, 66 (2002); A. V. Belitsky, X. Ji and F. Yuan, Nucl. Phys. B **656**, 165 (2003).
 - [7] D. Boer, P. J. Mulders and F. Pijlman, Nucl. Phys. B **667**, 201 (2003).

- [8] S. J. Brodsky, P. Hoyer, N. Marchal, S. Peigne and F. Sannino, *Phys. Rev. D* **65**, 114025 (2002).
- [9] E. Iancu, A. Leonidov and L. McLerran, arXiv:hep-ph/0202270; E. Iancu and R. Venugopalan, arXiv:hep-ph/0303204; J. Jalilian-Marian and Y. V. Kovchegov, *Prog. Part. Nucl. Phys.* **56**, 104 (2006); F. Gelis, E. Iancu, J. Jalilian-Marian and R. Venugopalan, arXiv:1002.0333 [hep-ph]; and references therein.
- [10] D. Boer and W. Vogelsang, *Phys. Rev. D* **69**, 094025 (2004).
- [11] C. J. Bomhof, P. J. Mulders and F. Pijlman, *Phys. Lett. B* **596**, 277 (2004); *Eur. Phys. J. C* **47**, 147 (2006); A. Bacchetta, C. J. Bomhof, P. J. Mulders and F. Pijlman, *Phys. Rev. D* **72**, 034030 (2005); C. J. Bomhof and P. J. Mulders, *JHEP* **0702**, 029 (2007).
- [12] J. W. Qiu, W. Vogelsang and F. Yuan, *Phys. Lett. B* **650**, 373 (2007); *Phys. Rev. D* **76**, 074029 (2007).
- [13] J. Collins and J. W. Qiu, *Phys. Rev. D* **75**, 114014 (2007).
- [14] W. Vogelsang and F. Yuan, *Phys. Rev. D* **76**, 094013 (2007); J. Collins, arXiv:0708.4410 [hep-ph].
- [15] T. C. Rogers and P. J. Mulders, *Phys. Rev. D* **81**, 094006 (2010) [arXiv:1001.2977 [hep-ph]].
- [16] B. W. Xiao and F. Yuan, *Phys. Rev. Lett.* **105**, 062001 (2010) [arXiv:1003.0482 [hep-ph]].
- [17] E. Braidot, for the STAR Collaboration, arXiv:1008.3989 [nucl-ex]; B. Meredith, for the PHENIX Collaboration, to appear;
- [18] see, for example, K. Hencken *et al.*, *Phys. Rept.* **458**, 1 (2008), and references therein.
- [19] L. D. McLerran and R. Venugopalan, *Phys. Rev. D* **49**, 2233 (1994) [arXiv:hep-ph/9309289]; *Phys. Rev. D* **49**, 3352 (1994) [arXiv:hep-ph/9311205].
- [20] S. Peigne, *Phys. Rev. D* **66**, 114011 (2002).
- [21] S. J. Brodsky, B. Pasquini, B. W. Xiao and F. Yuan, *Phys. Lett. B* **687**, 327 (2010) [arXiv:1001.1163 [hep-ph]].
- [22] A. H. Mueller, *Nucl. Phys. B* **415**, 373 (1994).
- [23] A. H. Mueller, arXiv:hep-ph/9911289.
- [24] F. Gelis and A. Peshier, *Nucl. Phys. A* **697**, 879 (2002) [arXiv:hep-ph/0107142].
- [25] J. P. Blaizot, F. Gelis and R. Venugopalan, *Nucl. Phys. A* **743**, 57 (2004) [arXiv:hep-ph/0402257].
- [26] K. Fukushima and Y. Hidaka, *JHEP* **0706**, 040 (2007) [arXiv:0704.2806 [hep-ph]].
- [27] A. H. Mueller, *Nucl. Phys. B* **558**, 285 (1999).
- [28] L. D. McLerran and R. Venugopalan, *Phys. Rev. D* **59**, 094002 (1999); R. Venugopalan, *Acta Phys. Polon. B* **30**, 3731 (1999).
- [29] C. Marquet, B. W. Xiao and F. Yuan, *Phys. Lett. B* **682**, 207 (2009). [arXiv:0906.1454 [hep-ph]].
- [30] M. Braun, *Eur. Phys. J. C* **16**, 337 (2000) [arXiv:hep-ph/0001268]; *Phys. Lett. B* **483**, 105 (2000) [arXiv:hep-ph/0003003].
- [31] D. Kharzeev, Y. V. Kovchegov and K. Tuchin, *Phys. Rev. D* **68**, 094013 (2003) [arXiv:hep-ph/0307037].
- [32] F. Dominguez, C. Marquet and B. Wu, *Nucl. Phys. A* **823**, 99 (2009) [arXiv:0812.3878 [nucl-th]].
- [33] C. Marquet, *Nucl. Phys. A* **796**, 41 (2007); J. L. Albacete and C. Marquet, arXiv:1005.4065 [hep-ph].
- [34] K. Tuchin, *Nucl. Phys. A* **846**, 83 (2010) [arXiv:0912.5479 [hep-ph]].
- [35] F. Dominguez, B. W. Xiao and F. Yuan, to be published.